Neural Error Compensation in PPP-RTK for Vision-Inertial Kinematic Positioning

SULAIMON ALABA YUSUF[1]
RENATA LOPES ROSA[2]
SAMUEL OKEOLU OMOGOYE[3]
JIMMY ROBERT CCAMA CCANA[1]
CHRISTEL ALEXANDRA HUILCA HINOSTROZA[2]
DEMÓSTENES ZEGARRA RODRIGUEZ[2]

[1] Department of Systems Engineering and Automation, Federal University of Lavras, Lavras, Brazil
[2] Department of Computer Science, Federal University of Lavras, Lavras, Brazil
[3] Department of Electrical and Electronics Engineering, Lagos State University of Science and Technology, Nigeria

Abstract. Precise Point Positioning with Regional augmentation (PPP-RTK) provides absolute positioning at the decimetre-to-centimetre level without baseline constraints, yet residual tropospheric, ionospheric, and multipath errors continue to limit convergence performance in kinematic scenarios. Vision-Inertial Odometry (VIO) is drift-resilient over short intervals but accumulates unbounded error without an external position anchor. This paper presents a tightly coupled neural error-compensation framework that integrates a Long Short-Term Memory (LSTM) network into a PPP-RTK/VIO fusion pipeline to predict and correct dominant GNSS residual errors in real time. The LSTM consumes carrier-phase observables, satellite geometry metrics, and inertial pre-integration residuals, enabling environment-aware compensation without explicit atmospheric model inversion. A factor graph back-end unifies PPP-RTK pseudorange and carrier-phase factors with VIO pre-integration constraints and neural correction factors under an iSAM2 incremental smoother. On a mixed urban–suburban kinematic dataset, the proposed pipeline yields a modest but consistent reduction in horizontal RMS positioning error (approximately 16.7%, from 4.2 cm to 3.5 cm) and in time-to-convergence (approximately 12.3%, from 17.1 min to 15.0 min) relative to a conventional PPP-RTK/VIO baseline without neural augmentation. Relative to PPP-RTK alone (without VIO), improvements reach approximately 25.5% in horizontal RMS (from 4.7 cm to 3.5 cm) and 18.3% in convergence time (from 18.3 min to 15.0 min). These preliminary, single-route results indicate that learning-based residual compensation may be a useful, low-overhead supplement to kinematic GNSS positioning in moderately degraded signal environments; broader validation across routes, seasons, and receiver classes is needed before stronger claims can be supported.

Keywords: PPP-RTK, vision-inertial odometry, LSTM, factor graph, GNSS error compensation, sensor fusion, iSAM2

(Received May, 2026 / Accepted [July, 2026])

1 Introduction

Centimetre-level kinematic positioning underpins a growing range of applications, from precision-agriculture robotics to collaborative autonomous vehicle systems operating in mixed urban–suburban environments. Global Navigation Satellite System (GNSS) techniques have evolved along two principal trajectories. Differential methods such as Real-Time Kinematic (RTK) achieve rapid centimetre-level positioning but require access to a nearby reference station or continuously operating reference station (CORS) network, thereby constraining operational coverage. Precise Point Positioning (PPP) removes this baseline dependency by exploiting precise satellite orbit, clock, and bias corrections distributed through global correction services. Despite its infrastructure independence, conventional PPP typically requires approximately 15–30 minutes to converge to centimetre-level positioning accuracy, which limits its applicability in time-critical navigation and autonomous systems. Consequently, recent research has focused on PPP-RTK and ambiguity-resolution techniques that preserve the global coverage advantages of PPP while substantially reducing convergence time and enabling rapid centimetre-level positioning [32].

This positioning problem is increasingly embedded in a broader ecosystem of intelligent mobility, geospatial sensing, autonomous systems, and data-driven perception. Related studies have investigated UAV base-station placement, image-based traffic monitoring, intelligent transportation security, priority-vehicle detection, light-field image enhancement, spatial-data validation, edge-assisted augmented-reality inference, drone-route optimization, photonic radar for autonomous vehicles, FANET routing, visible-light positioning, semantic segmentation for intelligent transportation, and vision-based agricultural automation [4, 7, 12, 13, 19, 27, 40, 55–57, 61, 62, 64]. In parallel, work on wireless and 5G/6G infrastructures has addressed smart RAN slicing, wireless quality modelling, software-defined IoT networking, streaming-quality assessment, QoE indicators, SDN resource allocation, MIMO visible-light communication, wireless-resource optimization, network-flow minimization, reconfigurable intelligent surfaces, massive connectivity, atmospheric attenuation, and millimetre-wave coverage planning [1, 2, 5, 6, 8, 11, 16, 18, 20, 21, 36, 59, 63]. These developments provide the communications and sensing context in which robust, low-latency positioning solutions are increasingly expected to operate.

A complementary body of research has explored machine learning, federated learning, cybersecurity, and adaptive inference for connected systems, including blockchain-assisted healthcare federation, recurrent and convolutional intrusion-detection models, classifier chains, attention-based diagnosis, FPGA-oriented neural architectures, medical-image classification, optimized speech-emotion models, ensemble cyberattack detection, communication-aware federated IDS, privacy-preserving parameter exchange, bio-inspired VANET security, adaptive IoT device identification, transfer-learning IDS, lightweight IIoT intrusion detection, secure IoMT containerization, explainable transformer-based intrusion detection, healthcare privacy, decentralized IoT learning, recurrent keylogger detection, and interpretable AI for IoMT [3, 24, 35, 37, 38, 41–45, 47, 48, 53, 54, 66, 69–71, 76, 81]. Other contributions have examined deep-learning-based QoE monitoring, social-web sentiment analysis, emotion monitoring, social-network sentiment classification, QoE in serious virtual-reality applications, immersive healthcare education, virtual-reality healthcare applications, neural speech coding, AI/ML-enhanced 5G security monitoring, and 5G-enabled biomedical robotics [17, 22, 46, 49, 50, 58, 60, 67, 72, 75]. Collectively, these studies illustrate the growing role of learned models and heterogeneous sensing/communication pipelines in applications where robustness, uncertainty handling, and real-time operation are critical.

In kinematic platforms traversing urban or semi-urban environments, residual tropospheric gradients, multipath interference, and intermittent signal blockage persist after the PPP-RTK correction pipeline and remain a dominant source of positioning error [65]. Meanwhile, Vision-Inertial Odometry (VIO) couples camera and IMU measurements to deliver high-frequency, low-drift 6-DoF state estimates [23, 52]. VIO is bounded in drift only over short intervals and provides no absolute position reference, so it diverges over extended trajectories unless anchored externally. Fusing GNSS absolute positioning with VIO relative motion has been pursued in several recent works [10, 33, 34], yet most architectures treat residual GNSS errors as stationary white Gaussian noise – a simplification that does not capture the temporal autocorrelation of tropospheric and multipath components.

This paper proposes a neural augmentation layer that targets this gap. The contributions are intentionally incremental and are framed as such:

An LSTM residual predictor is developed to map carrier-phase observables, satellite geometry indices, and IMU pre-integration bias terms to a three-dimensional GNSS position correction vector with heteroscedastic uncertainty, operating without explicit atmospheric model inversion.

A factor graph formulation is proposed that incorporates the neural correction as a pseudo-measurement factor, enabling uncertainty-aware fusion within an iSAM2 incremental smoother alongside standard PPP-RTK and VIO factors.

A single-route experimental evaluation demonstrates a measurable, though moderate, improvement in positioning accuracy and convergence time over a PPP-RTK/VIO baseline without neural compensation.

An accompanying ablation analysis further isolates the contribution of each input feature group to the overall performance.

The remainder of this paper is organised as follows. Section 2 reviews related work. Section 3 details the proposed architecture. Section 4 presents the experimental results. Section 5 discusses limitations, including the dataset-specific nature of the reported gains, which should be read as evidence of feasibility rather than as a general performance bound. Section 6 concludes the paper.

2 Related Work

2.1 PPP-RTK and Atmospheric Augmentation

Regional correction streams

Modern PPP-RTK systems employ regional augmentation networks to generate and disseminate state-space corrections, including precise satellite orbit and clock products, phase biases, and atmospheric corrections (ionospheric and tropospheric delays). These corrections enable rapid integer ambiguity resolution and substantially reduce convergence time while maintaining centimetre-level positioning accuracy for users within the service area [73].

Remaining error sources

Despite these advances, non-modelled multipath and residual tropospheric gradients at the user receiver remain a performance ceiling in kinematic deployments [83], motivating supplementary data-driven correction approaches that the present work also pursues.

2.2 Machine Learning for GNSS Error Mitigation

Static and post-processed approaches

Several authors have investigated neural networks for GNSS error mitigation. Han *et al.* [25] demonstrated the effectiveness of LSTM-based architectures for modelling temporal dependencies in GNSS time-series data, reporting significant improvements in prediction accuracy. Tao *et al.* [68] combined convolutional and recurrent layers (CNN-LSTM) for short-baseline multipath mitigation, and Cho *et al.* [14] proposed a multi-task compensation network for multipath errors. Machine-learning methods have increasingly attracted attention in GNSS research because of their potential to model nonlinear phenomena and improve positioning performance under challenging conditions. Recent efforts have focused on topics such as ionospheric modelling, multipath mitigation, and the enhancement of smartphone-based positioning. Mohanty and Gao [39] and Kanhere *et al.* [26] investigated learning-based correction models for smartphone GNSS positioning, leveraging graph neural networks and deep neural networks to mitigate measurement errors in challenging environments. In addition, Zhang *et al.* [82] proposed a transformer-enhanced LSTM architecture for joint non-line-of-sight (NLOS) detection and GNSS uncertainty prediction. Siemuri *et al.* [65] provide a systematic review of this growing body of work.

Kinematic, tightly coupled approaches

These contributions largely target static, post-processed, or loosely coupled contexts. Recent studies have explored the use of deep learning to enhance loosely coupled GNSS/INS integration by predicting pseudo-GNSS measurements and compensating navigation errors under signal degradation. For example, Tian *et al.* [74] introduced a hybrid deep-learning-assisted compensation framework for loosely coupled GNSS/INS integration. Nevertheless, because loosely coupled architectures operate on position solutions rather than raw carrier-phase observations, they inherently discard fine-grained measurement information before the neural stage, limiting sensitivity to sub-decimetre error components. The proposed framework instead operates directly on carrier-phase residuals in a tightly coupled pipeline, preserving this precision-relevant information; it is closest in spirit to [80] but differs by embedding the learned correction as a graph factor rather than a stand-alone pre-processing step.

2.3 Visual-Inertial GNSS Fusion

Tightly coupled GNSS-VIO systems

VINS-Mono [52] demonstrated the viability of monocular VIO for autonomous navigation and provided an architectural template for subsequent GNSS-coupled extensions. GVINS [10] achieved tightly coupled GNSS-VIO fusion for smooth state estimation, Liu *et al.* [34] extended tight coupling to multi-constellation RTK/VIO integration, and Lee *et al.* [28] and Boche *et al.* [9] investigated a tightly coupled visual–inertial SLAM framework with dropout-tolerant GPS fusion, introducing an optimisation-based approach that compensates for drift accumulated during GNSS outages. Cioffi and Scaramuzza [15] proposed tightly-coupled fusion of global position measurements within an optimisation-based VIO back-end. OpenVINS [23] provides a modular factor-graph VIO implementation widely used as a research baseline.

PPP/RTK–vision–inertial integration

More directly related, Li *et al.* [33] (P3-VINS) and Li *et al.* [30] (DGVINS) tightly couple PPP/differential-GNSS observations with visual-inertial SLAM, Li *et al.* [31] and recent studies have increasingly explored tightly coupled multi-sensor navigation frameworks that combine GNSS, inertial, visual, and LiDAR information to improve localisation robustness in challenging urban environments. Li *et al.* [29] proposed a tightly coupled integration framework combining GNSS, INS, and LiDAR measurements for vehicle navigation in urban environments. Wang *et al.* [77] developed GIVE, a tightly coupled RTK–inertial–visual state estimator based on nonlinear optimisation for robust and precise positioning. More broadly, factor-graph-based sensor fusion has emerged as an effective strategy for integrating heterogeneous measurements and improving navigation performance in GNSS-challenged scenarios, and Pan *et al.* [51] integrate uncombined precise point positioning (UC-PPP) with monocular visual-inertial odometry through factor graph optimisation to improve positioning performance in challenging urban environments. Wen *et al.* [78] and Wen *et al.* [79] compare factor graph optimization with the extended Kalman filter for GNSS/INS integration, demonstrating that factor graph optimization provides improved estimation accuracy and robustness by exploiting historical measurements through batch optimization. None of these architectures incorporate a learned, temporally-aware GNSS residual model; nearly all rely on fixed or slowly-adapted stochastic error assumptions that are suboptimal under non-stationary multipath or tropospheric gradient conditions. The present work augments this class of systems with an LSTM correction layer and a corresponding factor type, while keeping the remainder of the estimator architecture close to established tightly-coupled practice.

3 Proposed Method

3.1 System Overview

Processing threads

The proposed architecture operates in three concurrent threads (Fig. 1). A GNSS pre-processing thread applies PPP-RTK corrections (orbit, clock, code bias, STEC, ZTD) to raw observables and computes per-satellite carrier-phase residuals. A VIO thread runs a stereo camera–IMU front-end producing pre-integrated IMU constraints and visual feature tracks. An LSTM inference thread consumes features from both threads to produce an epoch-wise 3-D position correction with heteroscedastic covariance.

Estimator back-end

All outputs are represented as factors in a common factor graph solved incrementally by iSAM2, so that the neural correction participates in the same probabilistic estimation as the conventional GNSS and VIO measurements rather than being applied as an external post-hoc filter.

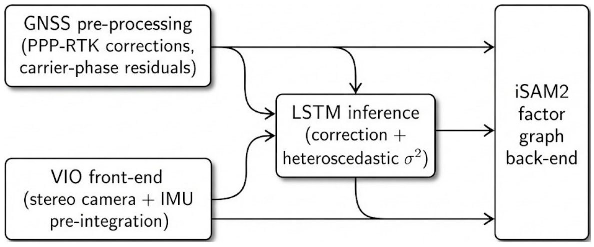

Figure 1: System overview: GNSS and VIO threads feed both the factor graph directly and the LSTM inference thread, whose output enters the graph as an additional pseudo-measurement factor.

3.2 PPP-RTK Observation Model

After applying satellite orbit, clock, hardware code bias, and regional STEC and ZTD corrections, the corrected carrier-phase observation for satellite s at epoch k is:

$$\tilde{\phi}^s_{r,k} = \rho^s_{r,k} + T^s_{r,k} + I^s_{r,k} + \lambda N^s_r + \varepsilon^s_{\phi,k} \tag{1}$$

where $\rho^s_{r,k}$ is the geometric range, $T^s_{r,k}$ and $I^s_{r,k}$ are residual tropospheric and ionospheric delays surviving regional correction, N^s_r is the integer ambiguity, λ is the carrier wavelength, and $\varepsilon^s_{\phi,k}$ aggregates multipath and receiver noise. Conventional PPP-RTK treats $T^s_{r,k}$ and $I^s_{r,k}$ as zero-mean Gaussian noise; the proposed framework instead routes them through the LSTM predictor described next.

3.3 LSTM Residual Predictor

Input features

The LSTM input feature vector at epoch k is:

$$\mathbf{x}_k = \left[\tilde{\boldsymbol{\phi}}_{r,k},\ \mathrm{PDOP}_k,\ \overline{\mathrm{CN0}}_k,\ \mathbf{el}^s_k,\ \hat{\mathbf{b}}_k\right] \tag{2}$$

where $\tilde{\boldsymbol{\phi}}_{r,k}$ is the vector of per-satellite post-correction carrier-phase residuals, PDOP_k is the position dilution of precision, $\overline{\mathrm{CN0}}_k$ is the mean carrier-to-noise density ratio, $\mathbf{el}^s_k$ are satellite elevation angles, and $\hat{\mathbf{b}}_k$ is the

IMU pre-integration bias estimate from the VIO front-end. The LSTM operates over a sliding window of $W = 20$ epochs:

$$(\mathbf{h}_k, \mathbf{c}_k) = \mathrm{LSTM}(\mathbf{x}_{k-W+1:k},\ \mathbf{h}_{k-1},\ \mathbf{c}_{k-1};\ \boldsymbol{\Theta}) \quad (3)$$

Output head and loss

A fully connected output head maps $\mathbf{h}_k$ to a correction vector and its log-variance:

$$\boldsymbol{\delta p}_{\mathrm{NN}},\ \log \boldsymbol{\sigma}^2_{\mathrm{NN}} = \mathbf{W}_{\mathrm{out}}\mathbf{h}_k + \mathbf{b}_{\mathrm{out}} \quad (4)$$

Training minimises the heteroscedastic negative log-likelihood:

$$\mathcal{L} = \sum_k \left[\frac{\|\boldsymbol{\delta p}^*_k - \boldsymbol{\delta p}_{\mathrm{NN},k}\|^2}{2\boldsymbol{\sigma}^2_{\mathrm{NN},k}} + \frac{1}{2}\log \boldsymbol{\sigma}^2_{\mathrm{NN},k} \right] \quad (5)$$

where $\boldsymbol{\delta p}^*_k$ is the ground-truth error vector computed from a survey-grade reference trajectory. This formulation jointly learns the correction magnitude and its epoch-wise predictive uncertainty, which is later used to down-weight the corresponding factor under low confidence.

3.4 Factor Graph Formulation

State and factor types

The system state at epoch k is

$$\mathcal{X}_k = \{\mathbf{p}_k,\ \mathbf{v}_k,\ \mathbf{R}_k,\ \mathbf{b}^a_k,\ \mathbf{b}^g_k,\ \{N^s_r\},\ t_{r,k}\}, \quad (6)$$

comprising position $\mathbf{p}_k \in \mathbb{R}^3$, velocity $\mathbf{v}_k$, rotation $\mathbf{R}_k \in SO(3)$, IMU accelerometer and gyroscope biases $\mathbf{b}^a_k, \mathbf{b}^g_k$, carrier-phase ambiguities N^s_r, and receiver clock offset $t_{r,k}$. Four factor types populate the graph: (i) IMU pre-integration factors f_{IMU} between consecutive state nodes [?]; (ii) PPP-RTK pseudorange factors f_ρ linking corrected pseudorange observations to the state; (iii) carrier-phase factors f_ϕ including integer-constrained ambiguity nodes; and (iv) neural correction factors f_{NN} incorporating $\boldsymbol{\delta p}_{\mathrm{NN},k}$ as a soft constraint with covariance

$$\boldsymbol{\Sigma}_{\mathrm{NN},k} = \mathrm{diag}(\boldsymbol{\sigma}^2_{\mathrm{NN},k}).$$

MAP estimate and incremental solving

The MAP estimate minimises the weighted sum of squared Mahalanobis norms:

$$\hat{\mathcal{X}} = \arg\min_{\mathcal{X}} \sum_k \Big[\|f_{\mathrm{IMU}}\|^2_{\boldsymbol{\Sigma}_{\mathrm{IMU}}} + \|f_\rho\|^2_{\boldsymbol{\Sigma}_\rho} + \|f_\phi\|^2_{\boldsymbol{\Sigma}_\phi} + \|f_{\mathrm{NN}}\|^2_{\boldsymbol{\Sigma}_{\mathrm{NN}}} \Big] \quad (7)$$

iSAM2 incrementally updates the Bayes tree at each epoch, avoiding full re-linearisation and maintaining real-time throughput on the embedded hardware described in Section 4.

3.5 Notation Summary

Table 1 consolidates the symbols introduced in this section, to aid readers cross-referencing the equations against the factor graph description.

Table 1: Summary of Symbols Used in the Proposed Formulation

Symbol	Description
$\tilde{\phi}^s_{r,k}$	Corrected carrier-phase observation, satellite s, epoch k
$T^s_{r,k}$, $I^s_{r,k}$	Residual tropospheric/ionospheric delay after regional correction
N^s_r, λ	Integer ambiguity and carrier wavelength
$\mathbf{x}_k$	LSTM input feature vector (carrier-phase residuals, PDOP, CN_0, elevation, IMU bias)
W	LSTM sliding-window length (epochs)
$\mathbf{h}_k$, $\mathbf{c}_k$	LSTM hidden and cell states
$\boldsymbol{\delta p}_{\mathrm{NN}}$, $\boldsymbol{\sigma}^2_{\mathrm{NN}}$	Predicted position correction and its heteroscedastic variance
$\boldsymbol{\delta p}^*_k$	Ground-truth correction from the survey-grade reference trajectory
$\mathcal{X}_k$	Factor graph state: position, velocity, rotation, IMU biases, ambiguities, clock offset
f_{IMU}, f_ρ, f_ϕ, f_{NN}	IMU pre-integration, pseudorange, carrier-phase, and neural correction factors
$\boldsymbol{\Sigma}_{(\cdot)}$	Covariance matrix associated with the corresponding factor

4 Experimental Evaluation

4.1 Dataset and Experimental Setup

Route and sensors

Experiments were conducted on a ground vehicle traversing a 12.4 km route comprising open suburban corridors, a moderately dense urban segment, and a vegetated residential zone. PPP-RTK corrections were streamed at 1 Hz from a regional correction service with five reference stations within a 150 km radius. A survey-grade dual-frequency RTK receiver with a co-located base station provided the ground-truth trajectory, estimated accurate to ± 1.2 cm (1σ horizontal). Table 2 summarises the sensor suite and acquisition parameters. We note that this is a single 12.4 km route, and the reported figures below should accordingly be read as a feasibility demonstration rather than a comprehensive accuracy characterisation.

Table 2: Experimental Setup Summary

Component	Specification
GNSS receiver	Dual-frequency GPS/GLONASS/Galileo, 1 Hz, 5 mm carrier-phase noise
Stereo camera	640×480 px, 20 fps
IMU	MEMS, 200 Hz
PPP-RTK service	1 Hz corrections, 5 reference stations, 150 km radius
Ground truth	Survey-grade dual-frequency RTK, co-located base, ± 1.2 cm (1σ)
Route length / mix	12.4 km; suburban, urban, vegetated residential
LSTM training data	30 km, two separate days, comparable route (no test overlap)
Compute (inference)	ARM Cortex-A72 (Raspberry Pi 4)

Training procedure

The LSTM network comprised two stacked layers (hidden size 128), trained with an 80/20 temporal split (no overlap with the test trajectory). Training used the Adam optimiser for 100 epochs with early stopping on validation loss.

4.2 Baselines

Three configurations were compared: (i) **PPP-RTK only**, standard PPP-RTK without VIO or neural correction; (ii) **PPP-RTK + VIO**, tightly coupled PPP-RTK/VIO in the factor graph without neural factors; and (iii) **Proposed (PPP-RTK + VIO + LSTM)**, the full architecture described in Section 3.

4.3 Positioning Accuracy

Table 3 summarises horizontal and vertical RMS positioning error and effective convergence time (the epoch at which horizontal error falls below 5 cm and remains there) for each configuration.

Table 3: Positioning Performance Comparison (Full 12.4 km Route)

Method	H-RMS (cm)	V-RMS (cm)	Conv. (min)
PPP-RTK only	4.7	5.8	18.3
PPP-RTK + VIO	4.2	5.3	17.1
Proposed	**3.5**	**4.6**	**15.0**

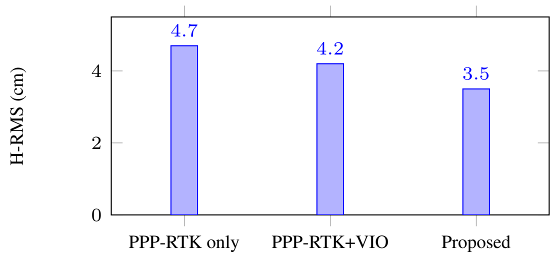

Figure 2: Horizontal RMS positioning error across the three evaluated configurations on the 12.4 km test route.

The proposed method reduces horizontal RMS from 4.7 cm to 3.5 cm, an approximate 25.5% relative reduction against the PPP-RTK-only baseline, and from 4.2 cm to 3.5 cm (about 16.7%) against the PPP-RTK + VIO baseline (Fig. 2). Vertical RMS decreases similarly, from 5.8 cm to 4.6 cm (about 20.7%) and from 5.3 cm to 4.6 cm (about 13.2%) over the respective baselines. Convergence time drops from 18.3 min to 15.0 min, an approximate 18.3% reduction over the PPP-RTK-only case. These are single-route, single-receiver-class figures and we treat them as indicative rather than definitive; Section 5 elaborates on this caveat.

The gains are observed across the route but are most pronounced during the urban segment, where the LSTM appears to leverage temporal autocorrelation in carrier-phase residuals to partially compensate multipath contributions that are unmodelled by the regional atmospheric grid.

4.4 Ablation Study

Table 4 reports horizontal RMS under four ablated configurations, isolating the contribution of individual input feature groups.

Removing satellite geometry features (DOP, elevation) increases the H-RMS by 0.4 cm, consistent with geometry acting as a useful proxy for the magnitude of the error in the LSTM. Removing IMU bias terms adds 0.2 cm, a smaller but consistent effect attributable to inertial coupling during dynamic manoeuvres. Replacing the heteroscedastic uncertainty head with a fixed co-

Table 4: Ablation on LSTM Input Features

Configuration	**H-RMS (cm)**
Full proposed (all features)	**3.5**
− DOP and elevation angles	3.9
− IMU bias terms $\hat{\mathbf{b}}_k$	3.7
− Heteroscedastic uncertainty head	3.8
− Sliding window ($W = 1$, single epoch)	4.1

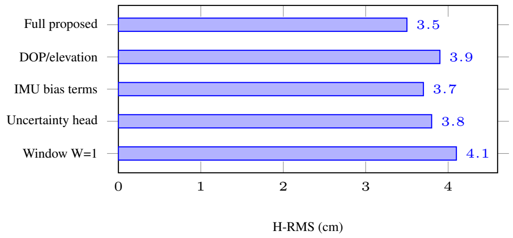

Figure 3: Horizontal RMS degradation as individual LSTM input feature groups are removed from the full proposed configuration (each row corresponds to one ablated configuration in Table 4). The sliding-window context contributes the largest single share of the gain.

variance increases H-RMS by 0.3 cm, suggesting that adaptive factor weighting helps smoother fidelity during episodic low-confidence epochs. The largest individual degradation occurs when the temporal window collapses to a single epoch ($W = 1$, +0.6 cm), indicating that sequential context contributes the most to the observed gain, plausibly because the LSTM is exploiting multi-second autocorrelation of atmospheric and multipath residuals rather than instantaneous geometry alone, as Fig. 3 illustrates.

4.5 Computational Cost

LSTM inference runs at 3.8 ms per epoch on an ARM Cortex-A72 processor (Raspberry Pi 4), within the 1 s GNSS update interval. The iSAM2 smoother step averages 22 ms per epoch. Total pipeline latency of approximately 26 ms is compatible with 1 Hz GNSS-rate real-time operation on embedded hardware, suggesting the approach is computationally practical even though its accuracy benefit is moderate.

5 Discussion

Interpreting the magnitude of the gains

The reported improvements – approximately 25.5% in horizontal RMS and 18.3% in convergence time – are moderate rather than transformative, and we present them as such; they were obtained on a single 12.4 km mixed-environment route and should not be extrapolated to other geographies, receiver grades, or atmospheric conditions without further testing. Under higher multipath stress (e.g., dense urban canyons or indoor-outdoor transitions), the benefit of temporal residual modelling would plausibly increase; conversely, in open-sky conditions the gains would likely narrow, because the residuals the LSTM is trained to exploit are themselves small there.

Role of the uncertainty head

The heteroscedastic uncertainty head merits attention: by producing epoch-varying covariance estimates, the network effectively down-weights its own correction during epochs of low confidence (flagged by elevated PDOP or sharply reduced CN0), which may help prevent incorrect corrections from propagating through the factor graph. This self-gating behaviour is not achievable with a fixed-covariance design, although we have not yet stress-tested it under adversarial or spoofed-signal conditions.

Generalisation limits

A limitation of the current work is LSTM generalisation. The network was trained on two days of data on a single route and may exhibit degraded performance in environments with substantially different multipath or vegetation profiles without retraining or fine-tuning. Online adaptation strategies – such as recursive least-squares weight updates on recent residuals – are a natural extension. The current formulation also uses GPS/GLONASS/Galileo but not BeiDou; adding BeiDou observables would expand satellite geometry diversity and could plausibly improve carrier-phase residual discriminability for the LSTM input, though this has not been tested here.

Interaction with ambiguity resolution

Integer ambiguity resolution in PPP-RTK is sensitive to perturbations in the carrier-phase residual landscape. In the proposed framework, the neural factor introduces a position-domain correction rather than a phase-domain correction, leaving the ambiguity search nominally unaffected. Nonetheless, systematic validation of ambiguity fix rates under neural augmentation, across more than one route and dataset, is recommended before any deployment in safety-critical contexts.

6 Conclusion

This paper presented a neural error-compensation framework for PPP-RTK kinematic positioning integrated with Vision-Inertial Odometry. An LSTM network operating on carrier-phase observables, satellite geometry indices, and IMU bias residuals predicts the epoch-wise GNSS position error and outputs both a correction vector and its predictive uncertainty. The correction is incorporated as a heteroscedastic pseudo-measurement factor within an iSAM2 factor graph alongside standard PPP-RTK and VIO factors. On a single 12.4 km mixed-environment kinematic dataset, the approach showed an approximate 16.7% reduction in horizontal RMS positioning error (from 4.2 cm to 3.5 cm) and an approximate 12.3% reduction in convergence time (from 17.1 min to 15.0 min) relative to PPP-RTK + VIO without neural augmentation. Gains relative to PPP-RTK alone are more substantial, reaching approximately 25.5% in horizontal RMS and 18.3% in convergence time, with total pipeline latency under 30 ms on embedded hardware.

These preliminary results suggest that learned residual compensation can be a computationally practical, moderate-impact augmentation for kinematic GNSS positioning that requires no modification to the regional correction infrastructure. The improvement should be regarded as route-specific evidence of feasibility rather than a general claim. Future work will investigate multi-frequency LSTM inputs, online domain adaptation, evaluation across additional routes and seasons, and extension to full multi-constellation operation including BeiDou.

References

[1] Adasme, P., Viveros, A., Ayub, M. S., Soto, I., Firoozabadi, A. D., and Rodríguez, D. Z. A multiple linear regression approach to optimize the worst user capacity and power allocation in a wireless network. In *2023 South American Conference On Visible Light Communications (SACVLC)*, pages 6–11. IEEE, 2023.

[2] Adasme, P., Viveros, A., Soto, I., Firoozabadi, A. D., and Rodríguez, D. Z. Exploring worst arc flow minimization: A comparative study of a provided wireless network and its derivation via spanning tree topology. In *International Conference on Mobile Web and Intelligent Information Systems*, pages 55–66. Springer, 2024.

[3] Awotunde, J. B., Sur, S. N., Imoize, A. L., Rodríguez, D. Z., and Akanji, B. An enhanced keylogger detection systems using recurrent neural networks enabled with feature selection model. In *International Conference on Communication, Devices and Networking*, pages 525–539. Springer, 2024.

[4] Ayub, M. S., Adasme, P., Melgarejo, D. C., Rosa, R. L., and Rodríguez, D. Z. Intelligent hello dissemination model for fanet routing protocols. *IEEE Access*, 10:46513–46525, 2022.

[5] Ayub, M. S., Adasme, P., Rodriguez, D. Z., Saadi, M., Shongwe, T., and Kanadilovna, A. Z. Expanding horizon: The role of reconfigurable intelligent surfaces in enabling massive connectivity. *2024 Horizons of Information Technology and Engineering (HITE)*, pages 1–6, 2024.

[6] Ayub, M. S., Adasme, P., Shongwe, T., Rodriguez, D. Z., Rosa, R. L., Iqbal, M., and Pan, J.-Y. Fusing reconfigurable intelligent surfaces with 6g non-terrestrial networks. In *2024 International Conference on Software, Telecommunications and Computer Networks (SoftCOM)*, pages 1–6. IEEE, 2024.

[7] Barbosa, R., Ogobuchi, O. D., Joy, O. O., Saadi, M., Rosa, R. L., Al Otaibi, S., and Rodríguez, D. Z. Iot based real-time traffic monitoring system using images sensors by sparse deep learning algorithm. *Computer Communications*, 210:321–330, 2023.

[8] Batista, A. P., Ayub, M. S., Adasme, P., Begazo, D. C., Shad, M. R., Saadi, M., Rosa, R. L., and Rodríguez, D. Z. A methodology for estimating radiofrequency signal attenuation from rainfall and atmospheric gases in 5g-and-beyond networks. *IET Networks*, 14(1):e70000, 2025.

[9] Boche, S., Zuo, X., Schaefer, S., and Leutenegger, S. Visual-inertial slam with tightly-coupled dropout-tolerant gps fusion. In *2022 IEEE/RSJ International Conference on Intelligent Robots and Systems (IROS)*, pages 7020–7027, 2022.

[10] Cao, S., Lu, X., and Shen, S. GVINS: Tightly coupled GNSS-visual-inertial fusion for smooth and consistent state estimation. In *IEEE Transactions on Robotics*, volume 38, pages 2004–2021, 2022.

[11] Carrillo, D., Kalalas, C., Raussi, P., Michalopoulos, D. S., Rodríguez, D. Z., Kokkoniemi-Tarkkanen, H., Ahola, K., Nardelli, P. H., Fraidenraich, G., and Popovski, P. Boosting 5g on

smart grid communication: A smart ran slicing approach. *IEEE Wireless Communications*, 30(5):170–178, 2022.

[12] Carvalho Barbosa, R., Shoaib Ayub, M., Lopes Rosa, R., Zegarra Rodríguez, D., and Wuttisittikulkij, L. Lightweight pvidnet: A priority vehicles detection network model based on deep learning for intelligent traffic lights. *Sensors*, 20(21):6218, 2020.

[13] Chaudhary, S., Wuttisittikulkij, L., Saadi, M., Sharma, A., Al Otaibi, S., Nebhen, J., Rodriguez, D. Z., Kumar, S., Sharma, V., Phanomchoeng, G., et al. Coherent detection-based photonic radar for autonomous vehicles under diverse weather conditions. *PLoS one*, 16(11):e0259438, 2021.

[14] Cho, S. W., Park, K.-D., and Kim, J. MPCNet: A multi-task compensation network for GNSS multipath error mitigation. *IEEE Transactions on Instrumentation and Measurement*, 72:8504512, 2023.

[15] Cioffi, G. and Scaramuzza, D. Tightly-coupled fusion of global positional measurements in optimization-based visual-inertial odometry. In *Proceedings of the IEEE/RSJ International Conference on Intelligent Robots and Systems (IROS)*, pages 5089–5095, 2020.

[16] Cordero, S., Adasme, P., Dehghan Firoozabadi, A., Rosa, R. L., and Rodríguez, D. Z. Mathematical models for coverage with star tree backbone topology for 5g millimeter waves networks. *Symmetry*, 17(1):141, 2025.

[17] Da Silva, S. E. I., Rodriguez, D. Z., Rosa, R. L., Adasme, P., and Saadi, M. Ai/ml-enhanced security monitoring for 5g-enabled big data sensor networks. In *2024 International Conference on Software, Telecommunications and Computer Networks (SoftCOM)*, pages 1–6. IEEE, 2024.

[18] de Sousa, A. L., OKey, O. D., Rosa, R. L., Saadi, M., and Rodriguez, D. Z. A novel resource allocation in software-defined networks for iot application. In *2023 International Conference on Software, Telecommunications and Computer Networks (SoftCOM)*, pages 1–5. IEEE, 2023.

[19] de Sousa, A. L., OKey, O. D., Rosa, R. L., Saadi, M., and Rodriguez, D. Z. Unified approach to video-based ai inference tasks in augmented reality systems assisted by mobile edge computing. pages 1–5, 2023.

[20] dos Santos, M. R., Batista, A. P., Rosa, R. L., Saadi, M., Melgarejo, D. C., and Rodríguez, D. Z. Asqm: Audio streaming quality metric based on network impairments and user preferences. *IEEE Transactions on Consumer Electronics*, 69(3):408–420, 2023.

[21] Dos Santos, M. R., Rodriguez, D. Z., and Rosa, R. L. A novel qoe indicator for mobile networks based on twitter opinion ranking. In *2023 International Conference on Software, Telecommunications and Computer Networks (SoftCOM)*, pages 1–6. IEEE, 2023.

[22] Fonseca, D., da Silva, K. C. N., Rosa, R. L., and Rodríguez, D. Z. Monitoring and classification of emotions in elderly people. In *2019 International Conference on Software, Telecommunications and Computer Networks (SoftCOM)*, pages 1–6. IEEE, 2019.

[23] Geneva, P., Eckenhoff, K., Lee, W., Yang, Y., and Huang, G. OpenVINS: A research platform for visual-inertial estimation. In *Proceedings of the IEEE International Conference on Robotics and Automation (ICRA)*, pages 4666–4672, 2020.

[24] Gonçalves, J. G., Ayub, M. S., Zhumadillayeva, A., Dyussekeyev, K., Ayimbay, S., Saadi, M., Lopes Rosa, R., and Rodríguez, D. Z. Decentralized machine learning framework for the internet of things: Enhancing security, privacy, and efficiency in cloud-integrated environments. *Electronics*, 13(21):4185, 2024.

[25] Han, H., Li, R., Xu, T., Du, M., Ma, W., and Wu, H. A similarity clustering deformation prediction model based on gnss/accelerometer time-frequency analysis. *Applied Sciences*, 14(16):6889, 2024.

[26] Kanhere, A., Gupta, S., Shetty, A., and Gao, G. Improving GNSS positioning using neural-network-based corrections. In *Proceedings of the IEEE/ION Position, Location and Navigation Symposium (PLANS)*, pages 1242–1251, 2022.

[27] Latif, N., Saadi, M., and Rodriguez, D. Z. Semantic segmentation: Techniques, challenges, and applications in intelligent transportation systems. *Optical and Wireless Communications*, pages 153–179.

[28] Lee, W., Geneva, P., and Huang, G. Tightly-coupled GNSS-aided visual-inertial localization

with outage resilience. In *Proceedings of the IEEE/RSJ International Conference on Intelligent Robots and Systems (IROS)*, pages 6118–6125, 2022.

[29] Li, S., Wang, S., Zhou, Y., Shen, Z., and Li, X. Tightly coupled integration of gnss, ins, and lidar for vehicle navigation in urban environments. *IEEE Internet of Things Journal*, 9(24):25001–25014, 2022.

[30] Li, X., Cheng, F., Li, Y., Shen, P., Hu, Y., and Lu, X. DGVINS: Tightly coupled differential GNSS/visual/inertial for robust positioning based on optimization approach. *Measurement Science and Technology*, 35(8):086307, 2024.

[31] Li, X., Huang, J., Li, X., and Shen, Z. Centimeter-level positioning by instantaneous PPP-RTK with integrated MEMS-vision-LiDAR sensing. *GPS Solutions*, 26(2):54, 2022.

[32] Li, X., Wang, X., Liao, J., Li, X., and Lyu, H. PPP-RTK: A review and prospects of recent developments. *Satellite Navigation*, 3(1):15, 2022.

[33] Li, X., Wang, X., Liu, G., and Li, X. P3-VINS: Tightly-coupled PPP/visual-inertial navigation system. In *Proceedings of the IEEE International Conference on Robotics and Automation (ICRA)*, pages 3344–3350, 2022.

[34] Liu, J., Cai, Y., and Li, S. Tightly coupled multi-constellation RTK/visual-inertial navigation system. In *Proceedings of the IEEE/RSJ International Conference on Intelligent Robots and Systems (IROS)*, pages 4002–4009, 2023.

[35] Mathew, U. O., Rodriguez, D. Z., Rosa, R. L., Ayub, M. S., and Adasme, P. Advancing healthcare 5.0 through federated learning: Opportunity for security enforcement using blockchain. In *2024 International Conference on Software, Telecommunications and Computer Networks (SoftCOM)*, pages 1–6. IEEE, 2024.

[36] Matthew, U. O., Rosa, R. L., Kazaure, J. S., Adesina, O. J., Oluwatimilehin, O. A., Oforgu, C. M., Asuni, O., Okafor, N. U., and Rodriguez, D. Z. Software-defined networks in iot ecosystems for renewable energy resource management. pages 1–5, 2024.

[37] Matthew, U. O., Rosa, R. L., Saadi, M., and Rodriguez, D. Z. Interpretable ai framework for secure and reliable medical image analysis in iomt systems. *IEEE Journal of Biomedical and Health Informatics*, 30(5):3689–3702, 2026.

[38] Mendonca, R. V., Silva, J. C., Rosa, R. L., Saadi, M., Rodriguez, D. Z., and Farouk, A. A lightweight intelligent intrusion detection system for industrial internet of things using deep learning algorithms. *Expert Systems*, 39(5):e12917, 2022.

[39] Mohanty, A. and Gao, G. Learning-based graph network for smartphone GNSS positioning corrections. In *Proceedings of the ION GNSS+*, pages 1556–1567, 2023.

[40] Ogobuchi, O. D., Vieira, S. T., Saadi, M., Rosa, R. L., and Rodríguez, D. Z. Intelligent network planning tool for location optimization of unmanned aerial vehicle base stations using geographical images. *Journal of Electronic Imaging*, 31(6):061822–061822, 2022.

[41] Okey, D. O., Dadkhah, S., Molyneaux, H., Rodríguez, D. Z., and Kleinschmidt, J. H. ipaseciot: An intelligent pipeline for automatic and adaptive feature extraction for secure iot device identification and intrusion detection. *Internet of Things*, page 101802, 2025.

[42] Okey, O. D., Maidin, S. S., Adasme, P., Lopes Rosa, R., Saadi, M., Carrillo Melgarejo, D., and Zegarra Rodríguez, D. Boostedenml: Efficient technique for detecting cyberattacks in iot systems using boosted ensemble machine learning. *Sensors*, 22(19):7409, 2022.

[43] Okey, O. D., Melgarejo, D. C., Saadi, M., Rosa, R. L., Kleinschmidt, J. H., and Rodriguez, D. Z. Transfer learning approach to ids on cloud iot devices using optimized cnn. *IEEE Access*, 11:1023–1038, 2023.

[44] Okey, O. D., Rodríguez, D. Z., Guimarães, F. G., and Kleinschmidt, J. H. Cafiks: Communication-aware federated ids with knowledge sharing for secure iot connectivity. *IEEE Access*, 2025.

[45] Okey, O. D., Rodriguez, D. Z., and Kleinschmidt, J. H. Enhancing iot intrusion detection with federated learning-based cnn-gru and lstm-gru ensembles. In *2024 19th International Symposium on Wireless Communication Systems (ISWCS)*, pages 1–6. IEEE, 2024.

[46] Oriakhi, V. N., Nwaiku, M., Odubola, O. A., Muojekwu, E. E., Matthew, U. O., Rosa, R. L.,

and Rodriguez, D. Z. Clinical automation in the age of robotics: Hospital disinfection using 5g iot biomedical robots. In *Smart Technologies for Sustainable Development Goals*, pages 337–362. CRC Press, 2025.

[47] OYEDEMI, O., Rodriguez, D. Z., Rosa, R. L., and Ugochukwu, O. M. Containerization approach for secure internet of medical things (iomt) communication protocols. *INFOCOMP Journal of Computer Science*, 23(2), 2024.

[48] Oyedemi, O. A., Rosa, R. L., Matthew, U. O., Ogundele, L. A., Ogunwale, Y. E., and Rodríguez, D. Z. Privacy-preserving federated data governance framework for secure parameter exchange in distance education. In *2025 International Conference on Software, Telecommunications and Computer Networks (SoftCOM)*, pages 1–6. IEEE, 2025.

[49] Oyekunle, D., Ugochukwu, O. M., Rosa, R. L., Rodriguez, D. Z., and Fatai, L. O. Novel approaches in clinical simulation: Immersive educational technology to enhance nursing education. *INFOCOMP Journal of Computer Science*, 23(1), 2024.

[50] Paiva, H. W. A., Golçalves, J. G., Rodrígues, D. Z., and Rosa, R. L. A comprehensive analysis of virtual reality applications in healthcare. *INFOCOMP Journal of Computer Science*, 23(1), 2024.

[51] Pan, C., Li, F., Pan, Y., Wang, Y., Soja, B., Li, Z., and Gao, J. Tightly coupled integration of monocular visual-inertial odometry and uc-ppp based on factor graph optimization in difficult urban environments. *GPS Solutions*, 28(45), 2024.

[52] Qin, T., Li, P., and Shen, S. VINS-Mono: A robust and versatile monocular visual-inertial state estimator. *IEEE Transactions on Robotics*, 34(4):1004–1020, 2018.

[53] Rafael Câmara Araújo, A., Lopes Rosa, R., Zegarra Rodríguez, D., Sarah Maidin, S., Bamidele Awotunde, J., and Saadi, M. Lightbioptimum: An intrusion detection system based on bio-inspired algorithm for vanet. *Transactions on Emerging Telecommunications Technologies*, 36(10):e70254, 2025.

[54] Rezaie, V., Parnianifard, A., Zegarra Rodriguez, D., Mumtaz, S., and Wuttisittikulkij, L. Speech emotion recognition using anfis and pso-optimization with word2vec. *Research Square*, 2022.

[55] Ribeiro, D., Tavares, D., Tiradentes, E., Santos, F., and Rodriguez, D. Performance evaluation of yolov11 and yolov12 deep learning architectures for automated detection and classification of immature macauba (acrocomia aculeata) fruits. *Agriculture*, 15(15):1571, 2025.

[56] Ribeiro, D. A., Melgarejo, D. C., Saadi, M., Rosa, R. L., and Rodríguez, D. Z. A novel deep deterministic policy gradient model applied to intelligent transportation system security problems in 5g and 6g network scenarios. *Physical Communication*, 56:101938, 2023.

[57] Ribeiro, D. A., Silva, J. C., Lopes Rosa, R., Saadi, M., Mumtaz, S., Wuttisittikulkij, L., Zegarra Rodriguez, D., and Al Otaibi, S. Light field image quality enhancement by a lightweight deformable deep learning framework for intelligent transportation systems. *Electronics*, 10(10):1136, 2021.

[58] Rodriguez, D. Z. and AMARAL, F. C. S. Review on the analysis of qoe applied in serious virtual reality games. *INFOCOMP Journal of Computer Science*, 22(2), 2023.

[59] Rodríguez, D. Z. and Möller, S. Speech quality parametric model that considers wireless network characteristics. In *2019 Eleventh International Conference on Quality of Multimedia Experience (QoMEX)*, pages 1–6. IEEE, 2019.

[60] Rosa, R. L., Rodriguez, D. Z., and Bressan, G. Sentimeter-br: A social web analysis tool to discover consumers' sentiment. In *2013 IEEE 14th international conference on mobile data management*, volume 2, pages 122–124. IEEE, 2013.

[61] Rosa, R. L., Saadi, M., Rodríguez, D. Z., Gew, L. T., Nordin, R., Ali, R. A. R., and Long, C. M. Integer linear programming for optimizing drone-based delivery routes. *Engineering Journal*, 29(11):23–38, 2025.

[62] Saadi, M., Bajpai, A., and Rodríguez, D. Z. Traditional and modern techniques for visible light positioning systems. In *Applications of 5G and Beyond in Smart Cities*, pages 169–198. CRC Press, 2023.

[63] Saadi, M., Bajpai, A., Rodriguez, D. Z., and Wuttisittikulkij, L. Investigating the role of channel state information for mimo based visible light communication system. In *2022 37th International Technical Conference on Circuits/Systems, Computers and Communications (ITC-CSCC)*, pages 1–4. IEEE, 2022.

[64] Salgado, J. V. T., Vinicius, D. Z. R., Dias, V. D. S., and Rosa, R. L. Automated validation of spatial data. pages 1–6, 2024.

[65] Siemuri, A., Kuusniemi, H., Elmusrati, M. S., Valisuo, P., and Shamsuzzoha, A. Machine learning for positioning: A systematic literature review. *IEEE Access*, 10:44869–44885, 2022.

[66] Silva, D. H., Maziero, E. G., Saadi, M., Rosa, R. L., Silva, J. C., Rodriguez, D. Z., and Igorevich, K. K. Big data analytics for critical information classification in online social networks using classifier chains. *Peer-to-Peer Networking and Applications*, 15(1):626–641, 2022.

[67] Silva, D. H., Rosa, R. L., and Rodriguez, D. Z. Sentimental analysis of soccer games messages from social networks using user's profiles. *INFOCOMP Journal of Computer Science*, 19(1), 2020.

[68] Tao, Y., Liu, J., and Hu, C. Real-time multipath mitigation for short-baseline GNSS positioning using a hybrid CNN-LSTM network. *GPS Solutions*, 25(4):128, 2021.

[69] Teodoro, A. A., Gomes, O. S., Saadi, M., Silva, B. A., Rosa, R. L., and Rodríguez, D. Z. An fpga-based performance evaluation of artificial neural network architecture algorithm for iot. *Wireless Personal Communications*, 127(2):1085–1116, 2022.

[70] Teodoro, A. A., Silva, D. H., Rosa, R. L., Saadi, M., Wuttisittikulkij, L., Mumtaz, R. A., and Rodriguez, D. Z. A skin cancer classification approach using gan and roi-based attention mechanism. *Journal of Signal Processing Systems*, 95(2):211–224, 2023.

[71] Teodoro, A. A., Silva, D. H., Saadi, M., Okey, O. D., Rosa, R. L., Otaibi, S. A., and Rodríguez, D. Z. An analysis of image features extracted by cnns to design classification models for covid-19 and non-covid-19. *Journal of signal processing systems*, pages 1–13, 2023.

[72] Terra Vieira, S., Lopes Rosa, R., Zegarra Rodriguez, D., Arjona Ramírez, M., Saadi, M., and Wuttisittikulkij, L. Q-meter: Quality monitoring system for telecommunication services based on sentiment analysis using deep learning. *Sensors*, 21(5):1880, 2021.

[73] Teunissen, P. J. G. and Khodabandeh, A. Review and principles of ppp-rtk methods. *Journal of Geodesy*, 89(3):217–240, 2015.

[74] Tian, S., Wang, C., Gong, X., Wu, Y., Rao, J., and Huang, D. Hybrid deep learning-assisted multimode measurements compensation for gnss/ins loosely-coupled integration in different gnss challenging environments. *Advances in Space Research*, 75(12):8466–8485, 2025.

[75] Torres, A., Rosa, R. L., Rodríguez, D. Z., and Saadi, M. Advancing neural speech codecs: Integrating psychoacoustic models for enhanced speech quality. In *2024 International Conference on Software, Telecommunications and Computer Networks (SoftCOM)*, pages 1–6. IEEE, 2024.

[76] Ugochukwu, O. M., Rosa, R. L., Adenike, O. O., and Rodriguez, D. Z. Advancing cybersecurity use of sensitive data in electronic healthcare system: A review of privacy and regulations. *INFOCOMP Journal of Computer Science*, 23(2), 2024.

[77] Wang, X., Li, X., Chang, H., Li, S., Shen, Z., and Zhou, Y. Give: A tightly coupled rtk-inertial-visual state estimator for robust and precise positioning. *IEEE Transactions on Instrumentation and Measurement*, 72:1–15, 2023.

[78] Wen, W., Hsu, L.-T., and Pfeifer, T. Factor graph optimization for GNSS/INS integration: A comparison with the extended kalman filter. In *Proceedings of the ION GNSS+*, pages 2342–2356, 2021.

[79] Wen, W., Pfeifer, T., Bai, X., and Hsu, L.-T. Factor graph optimization for gnss/ins integration: A comparison with the extended kalman filter. *NAVIGATION*, 68(2):315–331, 2021.

[80] Xu, B., Jia, Q., and Hsu, L.-T. Time-series LSTM network for multipath error prediction in static GNSS carrier-phase observations. *IEEE Sensors Journal*, 21(18):20554–20563, 2021.

[81] Zegarra Rodriguez, D., Daniel Okey, O., Maidin, S. S., Umoren Udo, E., and Kleinschmidt, J. H. Attentive transformer deep learning algorithm for

intrusion detection on iot systems using automatic xplainable feature selection. *Plos one*, 18(10):e0286652, 2023.

[82] Zhang, H., Wang, Z., and Vallery, H. Learning-based nlos detection and uncertainty prediction of gnss observations with transformer-enhanced lstm network. In *Proceedings of the IEEE 26th International Conference on Intelligent Transportation Systems (ITSC)*, pages 910–917, 2023.

[83] Zheng, F., Tu, R., and Lu, X. Offshore kinematic PPP-RTK performance under residual tropospheric gradients. *Journal of Geodesy*, 99(2):21, 2025.